IJASS

International Journal of
Aeronautical and Space Sciences

Finite Volume Analysis of a Supersonic Non-Equilibrium Flow Around an Axisymmetric Blunt Body

R. Haoui*

Department of Mechanical Engineering, University of Science and Technology, Algiers, Algeria

Abstract

The aim of this work is to analyze high temperature flows around an axisymmetric blunt body taking into account chemical and vibrational non-equilibrium state for air mixture species. For this purpose, a finite volume methodology is employed to determine the supersonic flow parameters around the axisymmetric blunt body. This allows the capture of a shock wave before a blunt body placed in supersonic free stream. The numerical technique uses the flux vector splitting method of Van Leer. Here, adequate time stepping parameters, along with Courant, Friedrich, Lewis coefficient and mesh size level are selected to ensure numerical convergence, sought with an order of 10^{-8}.

Keywords: Supersonic flow, Non-equilibrium, Finite volume, Blunt body

Nomenclature

e_v	=	vibrational energy
K_f	=	forward reaction rate
K_b	=	backward reaction rate
K_{eq}	=	equilibrium constant
M	=	atomic mass
R	=	universal gas constant
r	=	constant of a particular gas
T	=	translational temperature
ω_{cs}	=	source term of chemical exchange
ω_{vs}	=	source term of production of vibration
A_s	=	species
v_s	=	stochiometric coefficients
p_s	=	density of species s
θ_d	=	characteristic temperature of dissociation
u, v	=	component velocity
p	=	pressure
e	=	energy per unit mass
$c_{v,t,r}$	=	translational and rotational specific heat at constant volume
Y_s	=	mass concentration of species s
$h_{f,s}^0$	=	enthalpy of formation
θ_v	=	characteristic temperature of vibration

1. Introduction

This article presents a calculation of a reactive flow around an axisymmetric blunt body in the shape of a hemisphere-cylinder. Experiments for the hypersonic shock tunnel remain a valuable source of information on the physicochemical phenomena that occur in the flow of air surrounding the model. Numerical simulations were used to supplement the theoretical and experimental studies. The simulations were performed by powerful calculators and powerful mathematical tools. In the present work, we implemented a numerical technique to simulate the hypersonic flow around an axisymmetric blunt body. The gas considered is the air in a standard state composed of 21% O_2 and 79% N_2. The infinite conditions of the flow are those of the atmosphere at a given altitude. In addition, it is necessary to take into account the air under a non-equilibrium state at the exit of a nozzle (Haoui at al., 2001).

Upstream the body, an intense detached shock wave occurred resulting in a very large temperature increase located at the nose of the body just after the shock. For this case, the air starts to dissociate and transforms into a gas composed of five species, O_2, N_2, NO, O, and N. There are several models that treat chemical kinetics that differ according to the number of chemical reactions. A realistic study must consider all the probable chemical reactions occurring in the flow. For this study, the model with seventeen chemical reactions is selected, 15 dissociation reactions and 2 exchange reactions (Haoui et al., 2001).

©*Corresponding author, E-mail: haoui_rabah@yahoo.fr

Speeds of the reactions employed are based on Arrhenius law. This is in addition to the expression of Landau and Teller (1936) for non-equilibrium of vibration. The time characteristic of vibration is given by the Blackman model (Blackman, 1955). The time characteristic of translation and rotation of molecules are very short in comparison to the time characteristic transition of the flow; however, the time it takes to return to the equilibrium state for these modes is very fast. Note that equilibrium of translation and rotation is carried out in any point of the flow and at any moment. By considering the range of temperatures in which the present study is placed, which is approximately 6,000 K, the phenomena of ionization of the species can be neglected. Similarly, effect of radiation is ignored. The chemical kinetics and the non-equilibrium of vibration are taken into account in the computational domain. The system of nonlinear partial derivative equations which governs this flow are solved by an explicit, unsteady numerical scheme (Goudjo and Desideri, 1989).

2. Equations

The Euler equations for the mixture in non-equilibrium contain mass conservation, momentum and energy equations of the evolution of chemical species (N_2, O_2, NO, O, N) and the energy of vibration of the molecules. It should be noted that only O_2 and N_2 species are considered in the non-equilibrium state. The NO molecule is studied under vibrational equilibrium. The time characteristic of vibration of this molecule is lower than that of O_2 by two orders of magnitude between the temperatures 3,000 K and 7,000 K (Wray, 1962).

In its vectorial form, the system of equations is written in 3D as follows:

$$\frac{\partial W}{\partial t} + div\ (f) = \Omega \qquad (1)$$

Where:

$$\vec{f} = F.\vec{i} + G.\vec{j} + H.\vec{k} \qquad (2)$$

The flux W, F, G, H and Ω are:

$$W = \begin{Bmatrix} \rho \\ \rho u \\ \rho v \\ \rho w \\ \rho e \\ \rho_s \\ (\rho_s e_{vs})_{O2,N2} \end{Bmatrix} \quad F = \begin{Bmatrix} \rho u \\ \rho u^2 + p \\ \rho uv \\ \rho uw \\ (\rho e + p)u \\ \rho_s u \\ (\rho_s e_{vs} u)_{O2,N2} \end{Bmatrix}$$

$$G = \begin{Bmatrix} \rho v \\ \rho uv \\ \rho v^2 + p \\ \rho vw \\ (\rho e + p)v \\ \rho_s v \\ (\rho_s e_{vs} v)_{O2,N2} \end{Bmatrix} \quad H = \begin{Bmatrix} \rho w \\ \rho uw \\ \rho vw \\ \rho w^2 + p \\ (\rho e + p)w \\ \rho_s w \\ (\rho_s e_{vs} w)_{O2,N2} \end{Bmatrix}$$

$$\Omega = \begin{Bmatrix} 0 \\ 0 \\ 0 \\ 0 \\ 0 \\ \omega_{cs} \\ (\omega_{vs})_{O2,N2} \end{Bmatrix}$$

The energy per unit of mass e is such as:

$$e = \sum_{s=1}^{5} c_{vs}T + \sum_{s=1}^{5} Y_s e_{vs} + \sum_{s=1}^{5} Y_s h_f^0 + \frac{1}{2}\left(u^2 + v^2 + w^2\right) \qquad (3)$$

h_f^0 is the enthalpy of formation of the species s in J/kg:

$$h_f^0(O) = 15.43\,10^6, \quad h_f^0(N) = 33.62\,10^6$$
$$h_f^0(NO) = 2.996\,10^6$$
$$h_f^0(O2) = h_f^0(N2) = 0$$

The pressure of the mixture is obtained by the equation of state:

$$\frac{p}{\rho} = r_m T \qquad (4)$$

Where

$$r_m = \frac{R}{M_m} \qquad (5)$$

The temperature of the mixture is calculated based on the energy Eq. (3). The source term of the chemical equation of evolution of species s is given by:

$$\omega_{cs} = M_s \sum_{r=1}^{r} (\upsilon_s'' - \upsilon_s') J_r \qquad (6)$$

Where:

$$J_r = K_f \prod_s \left(\frac{\rho_s}{M_s}\right)^{\upsilon_s'} - K_b \prod_s \left(\frac{\rho_s}{M_s}\right)^{\upsilon_s''} \qquad (7)$$

υ_s' and υ_s' are the stochiometric mole numbers of the reactants and products of species s, respectively, for each chemical reaction (r) such as:

$$\sum_s \upsilon'_s \, A_s \underset{K_b}{\overset{K_f}{\Leftrightarrow}} \sum_s \upsilon''_s \, A_s \quad \text{(Reaction r)} \quad (8)$$

Both forward and backward reaction rates are represented by K_f and K_b. An empirical expression for the forward reaction rate K_f may be written as

$$K_f = A \, T^n \exp\left(-\frac{T_d}{T}\right) \quad (9)$$

The backward reaction rate K_b is a function of the equilibrium constant K_{ep}

$$K_b = \frac{K_f}{K_{eq}} \quad (10)$$

The constants A, n and the temperature characteristic of dissociation T_d are given in Table 1 by Gardiner model (Gardiner, 1984). The equilibrium constant of the chemical reaction is given as a polynomial of the 4th degree:

Table 1. Forward constants (Gardiner models)

Reactions	A	n	T_d
r = 1	1.64 e+19	-1	59380
r = 2	3.64 e+18	-1	59380
r = 3	1.82 e+18	-1	59380
r = 4	4.56 e+19	-1	59380
r = 5	1.82 e+18	-1	59380
r = 6	1.40 e+21	-1.6	113200
r = 7	3.70 e+21	-1.6	113200
r = 8	1.40 e+21	-1.6	113200
r = 9	1.40 e+21	-1.6	113200
r = 10	60 e+22	-1.6	113200
r = 11	4.00 e+20	-1.5	75510
r = 12	4.00 e+20	-1.5	75510
r = 13	8.00 e+20	-1.5	75510
r = 14	8.00 e+20	-1.5	75510
r = 15	8.00 e+20	-1.5	75510
r = 16	1.82 e+14	0	38370
r = 17	3.80 e+9	1	20820

Table 2. Equilibrium constants

Reactions	c_0	c_1	c_2	c_3	c_4
r = 1 à 5	1.335	-4.127	-0.616	0.093	-0.005
r = 6 à 10	3.898	-12.611	0.683	-0.118	0.006
r = 11 à 15	1.549	-7.784	0.228	-0.043	0.002
r = 16	2.349	-4.828	0.455	-0.075	0.004
r = 17	0.215	-3.658	0.843	-0.136	0.007

$$K_{eq} = \exp(c_0 + c_1 z + c_2 z^2 + c_3 z^3 + c_4 z^4) \quad (11)$$

Where $z = \dfrac{10000}{T}$, and the coefficients c_0 through c_4 are provided for each reaction (Table 2).

The term of energy production of vibration ω_{vs} is:

$$\omega_{vs} = \rho_s \frac{e_v(T) - e_v(T_v)}{\tau_s} + e_{vs} \omega_{cs} \quad (12)$$

where $e_v(T)$ is the equilibrium energy of vibration at the temperature of translation-rotation, which is expressed as:

$$e_v(T) = \frac{r.\theta_v}{\exp(\frac{\theta_v}{T}) - 1} \quad (13)$$

where r is the constant of a particular gas and θ_v is the temperature characteristic of vibration. It is specified for each molecule. In the present work:

$$\theta_{vO2} = 2239K \quad \theta_{vN2} = 3354K$$
$$\theta_{vNO} = 2720K \quad (14)$$

$e_v(T_v)$ is the energy at the temperature of vibration T_v.

The time characteristic of vibration of a species s in the mixture τ_s is a function of the temperature, the pressure and the molar fractions X_i. It can be calculated as follows (Lee, 1986):

$$\frac{1}{\tau_s} = \sum_{i=1}^{5} \frac{X_i}{\tau_{s,i}} \quad (15)$$

Where $s = O_2, N_2$ and $i = O_2, N_2, NO, O, N \cdot \tau_{s,j}$ is the time characteristic of vibration of the species s in a mixture containing species i. We have:

$$\tau_{O2,O2} = \frac{1.692 10^{-9}}{p} \exp(101.44 \, T^{-1/3}) \quad (16)$$

$$\tau_{N2,N2} = \frac{1.1 10^{-11}}{p} T^{1/2} \exp(154.0 \, T^{-1/3}) \quad (17)$$

Experiments for binary exchanges, made it possible to evaluate vibrational relaxation time of O_2 in monatomic oxygen (Kiefer and Lutz, 1967) and of N_2 in O (Breshears and Bird, 1968), both correlated by (Thivet, 1989). The pressure p is in atmospheres and τ in seconds.
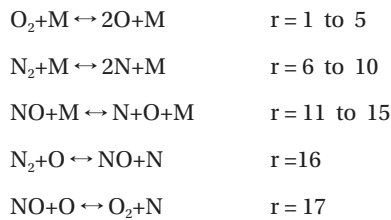
$$\tau_{O2,O} = \frac{T^{2/3}}{p} \exp(55.2 \, T^{-1/3} - 26.95) \quad (18)$$

61

$$\tau_{N2,O} = \frac{T^{2/3}}{p}\exp(70.3\,T^{-1/3} - 24.35) \qquad (19)$$

In order to determine the relaxation times, which are not given by the experimental correlations, it is supposed that the relaxation time of a species s is the same as the relaxation time of species i, provided that their masses are identical. Therefore, the following approximations can be employed:

$$\tau_{O2,N} \cong \tau_{O2,O} \qquad \tau_{N2,N} \cong \tau_{N2,O}$$

$$\tau_{O2,N2} \cong \tau_{O2,NO} \cong \tau_{O2,O2}$$

$$\tau_{N2,O2} \cong \tau_{N2,NO} \cong \tau_{N2,N2}$$

The model with 17 reactions is:

$O_2 + M \leftrightarrow 2O + M$	$r = 1$ to 5
$N_2 + M \leftrightarrow 2N + M$	$r = 6$ to 10
$NO + M \leftrightarrow N + O + M$	$r = 11$ to 15
$N_2 + O \leftrightarrow NO + N$	$r = 16$
$NO + O \leftrightarrow O_2 + N$	$r = 17$

M can be one of the five chemical species O_2, N_2, NO, O or N (in the order).

3. Axisymmetric Formulation

General information is not lost by seeking the solution at the points of an infinitely small domain Fig. 1. A method developed within the Sinus project of the National Institute of Research in Informatics and Automatic (NIRIA) Sophia-Antipolis (Goudjo and Desideri, 1989) makes it possible to pass from 3D to 2D axisymmetric model by using a technique of the disturbance of domain. By taking advantage of this finding, the problem is thus considered as axisymmetric.

The system of Eq. (1) can be written as:

$$\text{mes}(C_{i,j})\frac{\partial W_{i,j}}{\partial t} + \sum_{a\in\{x,x',y,y'\}}(F_{i,j}\vec{i} + G_{i,j}\vec{j}).\vec{\eta}_a -$$
$$H.\text{aire}(C_{i,j}) = \text{mes}(C_{i,j}).\Omega_{i,j} \qquad (20)$$

Where mes($C_{i,j}$) is the measurement (in m³) of an infinitely small volume of center (i, j). aire $(C_{i,j})$ is the surface of the symmetry plane passing by the center of an elementary volume. η_a is the integrated normal. For a detailed calculation of η_a, aire $(C_{i,j})$ and mes($C_{i,j}$), we refer to the work of (Goudjo and Desideri, 1989). The third term of the equation expresses the axisymmetric flow condition. Flows, W, F, G and H are given by:

$$W = \begin{Bmatrix} \rho \\ \rho u \\ \rho v \\ \rho e \\ \rho_s \\ (\rho_{vs}e_{vs})_{O2,N2} \end{Bmatrix} \qquad F = \begin{Bmatrix} \rho u \\ \rho u^2 + p \\ \rho uv \\ (\rho e + p)u \\ \rho_s u \\ (\rho_s e_{vs}u)_{O2,N2} \end{Bmatrix}$$

$$G = \begin{Bmatrix} \rho v \\ \rho uv \\ \rho v^2 + p \\ (\rho e + p)v \\ \rho_s v \\ (\rho_s e_{vs}v)_{O2,N2} \end{Bmatrix} \qquad H = \begin{Bmatrix} 0 \\ 0 \\ 2p \\ 0 \\ 0 \\ 0 \end{Bmatrix}$$

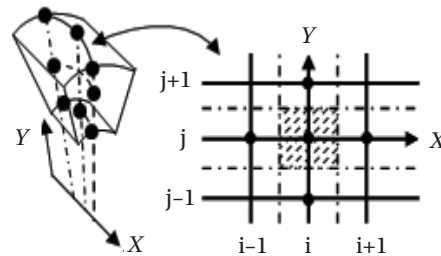$$\Omega = \begin{Bmatrix} 0 \\ 0 \\ 0 \\ 0 \\ \omega_{cs} \\ (\omega_{vs})_{O2,N2} \end{Bmatrix}$$

Fig. 1. Mesh form.

4. Discretization in Time

The present numerical method is based on an explicit approach in time and space. The step of time $\triangle t$ is as follows:

$$\triangle t = \min\left(\frac{\triangle x.CFL}{(\|V\| + a)}\right)_{i,j} \qquad (21)$$

The Courant, Friedrich, Lewis (CFL) is a stability factor. V is the velocity of the flow and a is the speed of sound. $\triangle x$ is the small length of the mesh at the same point (i, j). At each time step and for each point (i, j), the system of Eq. (20) can be written as

$$W_{i,j}^{n+1} = W_{i,j}^n - \frac{\Delta t}{\text{mes}(C_{i,j})}\sum_{a\in\{x,x',y,y'\}}(F_{i,j}^n\,\vec{i} + G_{i,j}^n\,\vec{j}).\vec{\eta}_a +$$
$$\Delta t\frac{\text{aire}(C_{i,j})}{\text{mes}(C_{i,j})}H_{i,j}^n + \Delta t.\Omega_{i,j}^n$$

$$(22)$$

The choice of the grid plays an important role in determining the convergence of the calculations. Therefore, it is indeed advisable to have sufficiently refined meshes at the places where the gradients of the flow parameters are significantly large, as observed in front of the nose of the obstacle.

5. Decomposition of Van-Leer

In this study, the decomposition of Van-Leer (1982) is selected, namely a decomposition of flow in two parts, F_{VL}^- and F_{VL}^+. This decomposition applies to the present two-dimensional problem by calculating the flow within each interface between two cells. Moreover, through this interface, the normal direction is paramount; thus, a reference mark is placed in the interface and the normal orientation is measured by an intermediate rotation, **R**, Fig. 2.
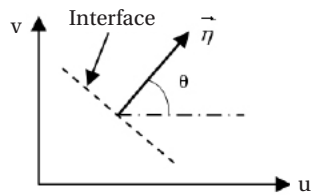
Fig. 2. Interface and its normal.

The vector W_E (Euler variable) is written W_E^R in the new reference mark

$$W_E^R = \begin{pmatrix} \rho \\ \rho \vec{V_n} \\ \rho e \end{pmatrix} \tag{23}$$

where $\vec{V_n}$ is obtained from $\vec{V}$, via the rotation **R**, in the following way:

$$\vec{V} = \begin{pmatrix} u \\ v \end{pmatrix} \rightarrow \vec{V_n} = \begin{pmatrix} u_n \\ v_n \end{pmatrix} = \begin{pmatrix} \cos\theta & \sin\theta \\ -\sin\theta & \cos\theta \end{pmatrix} \begin{pmatrix} u \\ v \end{pmatrix} \tag{24}$$

where:

$$\cos\theta = \frac{\eta_x}{\|\eta\|} \quad , \quad \sin\theta = \frac{\eta_y}{\|\eta\|} \tag{25}$$

$$\|\eta\| = \sqrt{\eta_x^2 + \eta_y^2} \tag{26}$$

The overall transformation **R** is

$$R = \begin{pmatrix} \cos\theta & \sin\theta \\ -\sin\theta & \cos\theta \end{pmatrix} \tag{27}$$

$$R^{-1} = \begin{pmatrix} \cos\theta & -\sin\theta \\ \sin\theta & \cos\theta \end{pmatrix} \tag{28}$$

Moreover, at each interface $(i+1/2)$, two neighbor states (i) and $(i+1)$ are known. Thus, one can calculate the one-dimensional flow, F, through the interface. The total flow, $f(W, \vec{\eta})$, may be deduced from F by applying the opposite rotation, as:

$$f(W, \vec{\eta}) = \|\eta\| R^{-1}\left(F(W^R)\right) \tag{29}$$

This property makes it possible to use only one component (F for example) of flow f to define the decomposition of flow in two dimensions. Moreover, this method is much easier and simpler to implement than the decomposition of flow in two dimensions $f = F.\eta_x + G\eta_y$.

The expressions of F_{VL}^+ and F_{VL}^- in 1-D, which are those of $F_{VL}^+(W^R)$ and $F_{VL}^-(W^R)$ by rotation R, where W^R is defined like the transform of W, can be written in the following from:

$$F_{VL}^+(W^R) = \begin{cases} F(W^R) & M_n \geq 1 \\ \begin{pmatrix} \dfrac{\rho a}{4}\left(\dfrac{u_n}{a}+1\right)^2 = f_1^+ \\ \dfrac{f_1^+}{\gamma}\left[(\gamma-1)u_n + 2a\right] \\ f_1^+ \cdot v_n \\ \dfrac{f_1^+}{2}\left[\dfrac{\left[(\gamma-1)u_n + 2a\right]^2}{\gamma^2-1} + v_n^2\right] \end{pmatrix} & |M_n| < 1 \\ 0 & M_n \leq -1 \end{cases} \tag{30}$$

$$F_{VL}^-(W^R) = \begin{cases} 0 & M_n \geq 1 \\ \begin{pmatrix} \dfrac{\rho a}{4}\left(\dfrac{u_n}{a}-1\right)^2 = f_1^- \\ \dfrac{f_1^-}{\gamma}\left[(\gamma-1)u_n - 2a\right] \\ f_1^- \cdot v_n \\ \dfrac{f_1^-}{2}\left[\dfrac{\left[(\gamma-1)u_n - 2a\right]^2}{\gamma^2-1} + v_n^2\right] \end{pmatrix} & |M_n| < 1 \\ F(W^R) & M_n \leq -1 \end{cases} \tag{31}$$

Where $M_n = \dfrac{u_n}{a}$, u_n and v_n are the velocity in the reference mark of the interface.

6. Boundary Conditions

6.1 Border Upstream

On the line of entrance, the parameters M, P, T and Y_s are fixed. Furthermore, as the flow reaches the entrance in

63

a supersonic state, these parameters are unchanged during the iterations.

6.2 Body Surface

Because flow is not viscous, a slip condition is applied to the wall. At any point, $M(x, y)$, on the wall the following condition must be checked:

$$\vec{V} . \vec{n} = 0 \tag{32}$$

where $\vec{n}$ is the normal to the wall.

6.3 Axis of Symmetry

In any point M of the axis of symmetry, the following condition should be satisfied:

$$v = 0 \quad \rightarrow \quad \vec{V} = u \vec{i} \tag{33}$$

6.4 Border Downstream

At the exit of the computational domain, which is downstream of the body, the flow is supersonic; the exit values of the flow filed parameters are extrapolated from the interior values.

7. Results and Interpretations

The body employed for the numerical simulations is a hemisphere followed by a cylinder with a 5° conical angle, as depicted in Fig. 3. The grid used in calculations is composed of 40×180 nodes. For illustration purposes, an example of grid with the dimensions 20×90 is presented in Fig. 4. The composition of the air of the upstream the flow is taken equal to 21% O_2 and 79% N_2. The pressure and the temperature related to the air at an altitude of 45 km, are 170 Pa and 295 K, respectively. The Mach number is set to 10. These values of the free stream correspond to the condition of spacecraft reentry into the Earth's atmosphere. Computations based on the 20×90 grid begin with the aerodynamic part, which converged after 1,000 iterations with a residue of 10^{-3}. This is followed by a complete scheme of simulations where the residue reaches 10^{-6} and number of iterations equals 2,600 iterations. Note that for the 40×180 grid, the iteration count increases to 5,400. The CFL is always taken equal to 0.4. For high precision we are used the 40×180 grid. The solution converges to the exact solution and the truncation error converges to zero, which confirms the consistency and the accuracy of our computer code, as shown in Fig. 5. For more details, see the Condition of convergence applied to an

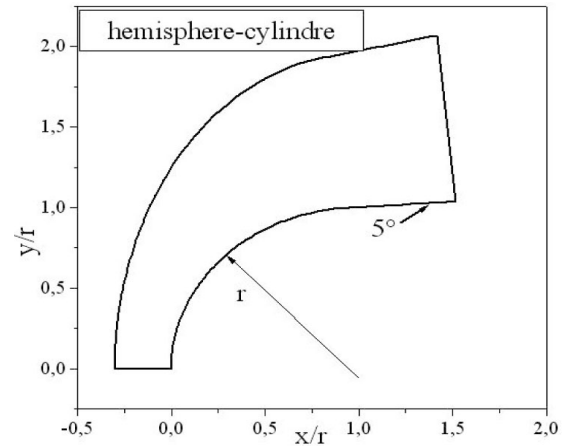axisymmetric reactive flow (Haoui et al., 2003).
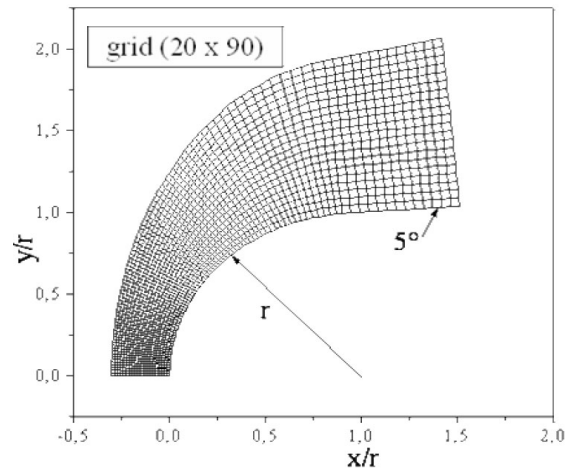

Fig. 3. Computational domain.
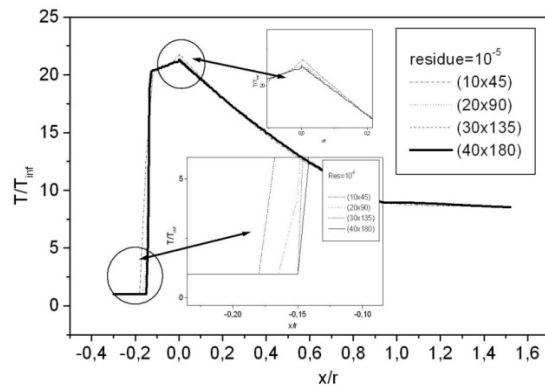

Fig. 4. Grid of (20×90).

Fig. 5. Grid convergence test, perfect gas.

For a flow neglecting the effects of thermo-chemistry, the mass fractions of the chemical species and the energy of vibration are supposedly fixed. The residue of the relative
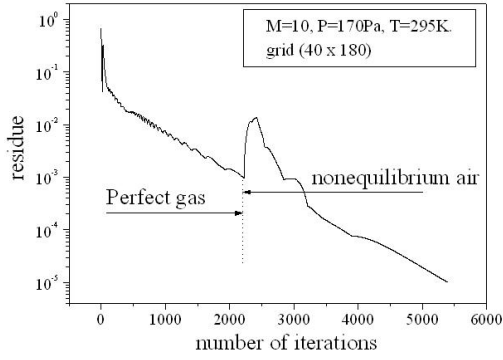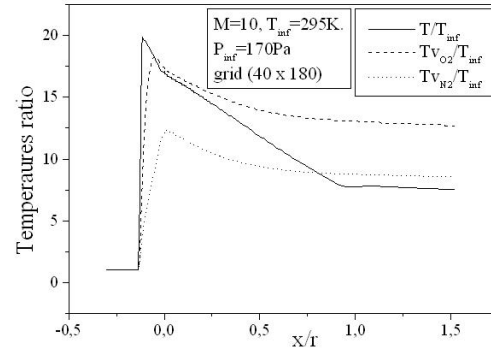
64

Fig. 6. Variation of residue.

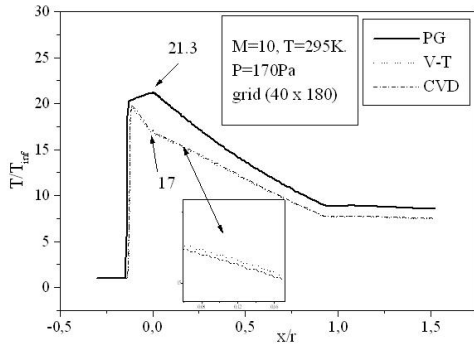Fig. 8. Variation of vibrational temperatures.

Fig. 7. Variation of translational-rotational temperatures. PG: perfect gas, CVD: coupling vibration-dissociation.
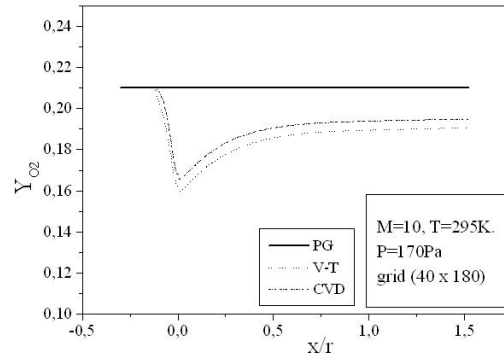

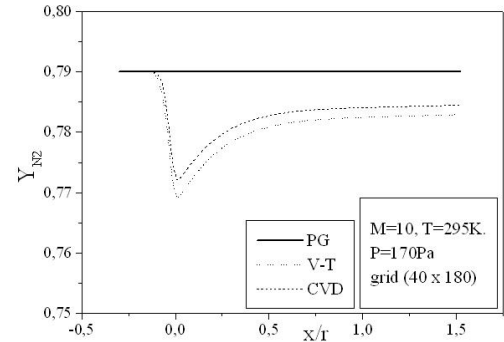Fig. 9. Evolution of the mass fraction of O_2. PG: perfect gas, CVD: coupling vibration-dissociation.

Fig. 10. Evolution of the mass fraction of N2. PG: perfect gas, CVD: coupling vibration-dissociation.

variation of the density is about 10^{-5}. There is no change in the findings for lower tolerance; Fig. 6 shows the variation of the residue according to the iterations count for a grid of 40 × 180 nodes. Figure 7 illustrates the variation of the temperature along the axis of symmetry until reaching a stagnation point, and then along the surface of the body. The difference between the cases of a perfect gas (PG), a non-equilibrium flow without coupling (V-T) and with coupling vibration-dissociation (CVD) according to the Park model (Park, 1989) while replacing the temperature t T in equation 9 by T^{1-q}. T_v^q where $q = 0.3$ are presented.

Temperatures obtained in the case of the reactive flow are lower than those of PG. At the stagnation point for example, the ratio of the temperature T of the flow to the temperature of free stream T_{inf} is 17 instead of 21.3. This is reduction of about **20.6%** in comparison to a PG. If we take into account the coupling CVD, the difference is weak between this case and the case without the coupling alternative.

Figure 8 depicts the variation of the temperature of vibration of O_2 and N_2 compared with the temperature of translation-rotation of the mixture. After the shock, the vibrational temperatures are strongly excited and after a distance of $\dfrac{x}{r} = 1$ becomes frozen, $T_{vO2}\big/T_{inf} = 12.7$, $T_{vN2}\big/T_{inf} = 8.55$ whereas $T\big/T_{inf} = 7.53$.
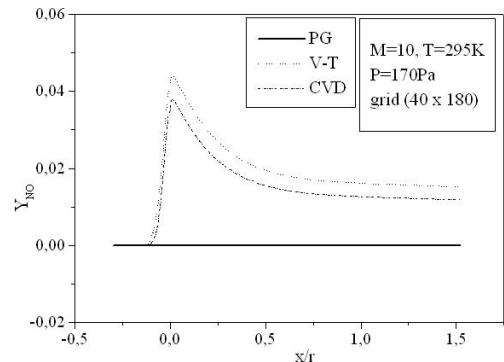

Fig. 11. Evolution of the mass fraction of NO. PG: perfect gas, CVD: coupling vibration-dissociation.
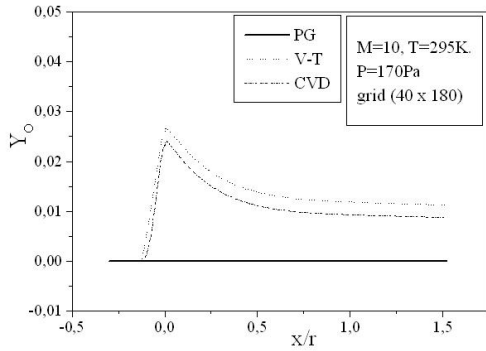
Fig. 12. Evolution of the mass fraction of O. PG: perfect gas, CVD: coupling vibration-dissociation.
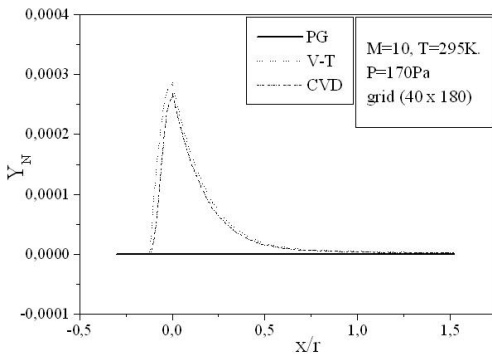

Fig. 13. Evolution of the mass fraction of N. PG: perfect gas, CVD: coupling vibration-dissociation.

Figures 9-13 illustrate the evolution of the mass fraction of the chemical species constituting the mixture of air. It is noticed that the dissociation of O_2 and N_2 starts just after the shock. Then, the concentrations decrease up to the stagnation point followed by a slow recombination because the velocity of the flow is larger compared to the chemical kinetics.

The mass fraction of the chemical species becomes frozen downstream where Y_{O_2} is equal to 0.19 instead of 0.21 and Y_{N_2} is equal to 0.78 instead of 0.79. For NO, O and N a fast formation of these species will occur after the shock up to the stagnation point and then a slow disappearance begins until having a freezing, where, $Y_{NO} = 1.16\%$, $Y_O = 0.9\%$ and $Y_N = 3.10^{-4}\%$.

Concerning the flow far from the wall, we presented the Mach-contours around the body in Fig. 14 where the shock wave detachment is visible in front of the nose of the body. The position of the detachment shock does not vary too much compared to the case without chemistry. For the non-equilibrium case, the position of the shock is at 0.135 times the radius in contrast to the case without chemistry (0.150 times the radius). Figure 15 shows the temperature-contours around the body. At the stagnation point the temperature is 5,015 K, whereas just after the shock it increases to 5,870 K; the difference is absorbed by the dissociation of the molecules. In addition, Figs. 16 and 17 depict the temperature-contours

of vibration of O_2 and N_2 providing a clear insight that the vibration is at non-equilibrium in the beginning and then it becomes frozen.
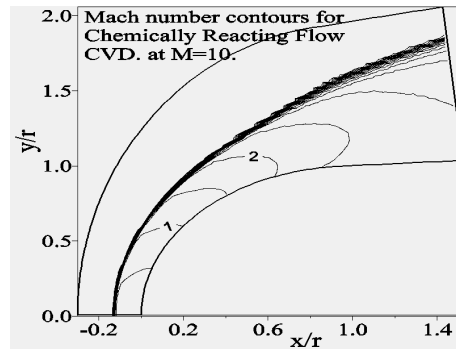

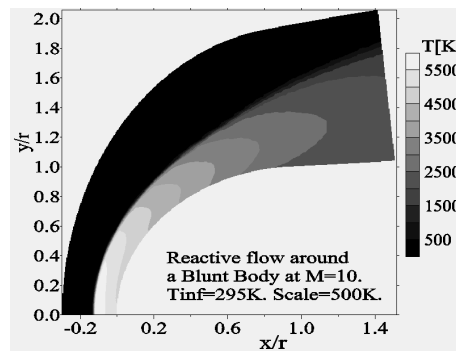Fig. 14. Mach number contours. CVD: coupling vibration-dissociation.
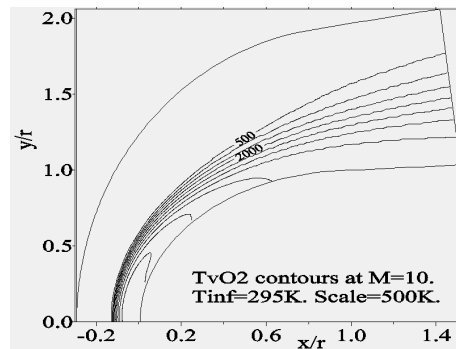

Fig. 15. Temperature contours.
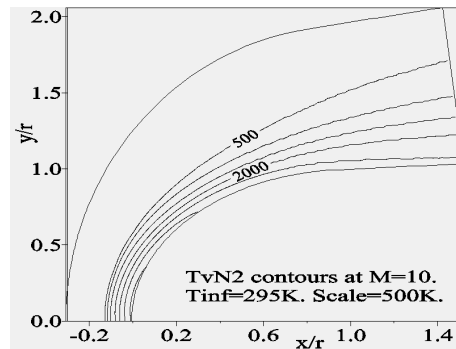

Fig. 16. Temperature contours of vibration of O2.

Fig. 17. Temperature contours of vibration of N2.
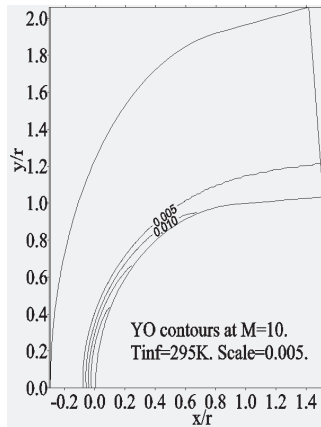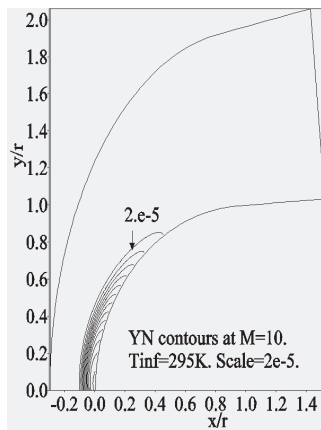
Fig. 18. Concentration contours of O.

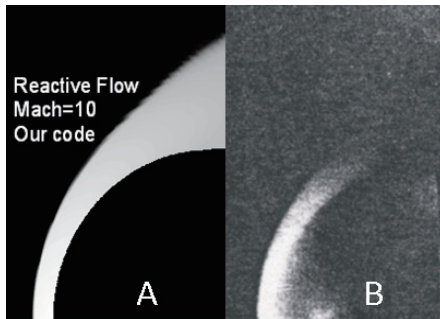Fig. 19. Concentration contours of N.

Fig. 20. Comparison computational-experimental: (a) Computational Mach contours; (b) test with a hemisphere model of a nominal Mach number 10 nozzle (Nagamatsu, 1959).

Furthermore, the concentration-contours of *O* and *N* are presented in Figs. 18 and 19. The reactive and frozen areas are clearly observed when one moves away from the stagnation point.

Due to the lack of experimental values in the literature, our results were compared with a real photograph of the same flow (Nagamatsu, 1959), Fig. 20. We can observe the position of the detached shock wave and the thickness of the reactive flow between the shock and the body.

8. Conclusions

The numerical simulation of flows around blunt bodies at high temperatures provided satisfactory results from a numerical and a physical point of view. With high degree of accuracy requirements, computational convergence is achieved and the physical phenomena considered are visible after the detached shock wave and around the blunt body. The choice of the kinetic model for this type of flows is interesting. The model with 17 reactions proves to be more realistic since it considers all the possible collisions between molecules and atoms of the mixture of air. After the shock, the air is in a state of non-equilibrium, and a frozen state is obtained after the stagnation point, from $x/_r = 0.6$ for the mass fractions and from $x/_r = 1$ for the vibration temperatures. At the node of the body, the temperature of gas is found to be lower in comparison to a model where the dissociations of molecules are not implemented in the simulation.

References

Blackman, V. H. (1955). *Vibrational Relaxation in Oxygen and Nitrogen (Technical Report)*. Palmer Physics Laboratory, Princeton University.

Breshears, W. D and Bird, P. F. (1968). Effects of oxygen atoms on the vibrational relaxation of nitrogen. *Journal of Chemical Physics*, 48, 4768-4773.

Burtschell, Y. (1990). *Performances, Dimensioning and Numerical Simulation of a Hypersonic Shock Tunnel with Reflected Shock of Free Piston*. PhD Thesis, University of Aix-Marseilles I, France.

Druguet, M. C. (1992). *Contribution to the Study of Nonequilibrium Reactive Hypersonic Euler's Flows*. PhD Thesis, University of Provence, France.

Gardiner, W. C. (1984). *Combustion Chemistry*. New-York: Springer-Verlag.

Goudjo, J. and Desideri, A. (1989). *A Finite Volume Scheme to Resolution an Axisymmetric Euler Equation*s. (Research Report INRIA 1005), National Institute of Research in Informatics and Automatic (NIRIA).

Haoui, R., Gahmousse, A., and Zeitoun, D. (2001). Chemical and vibrational nonequilibrium flow in a hypersonic axisymmetric nozzle. *International Journal of Thermal Sciences*, 40, 787-795.

Haoui, R., Gahmousse, A., and Zeitoun, D. (2003). Condition of convergence applied to an axisymmetric reactive flow. The *16th French Congress of Mechanic*, 1-5 September 2003, Nice, France, Paper 738.

Kiefer, J. H. and Lutz, R. W. (1967). The effect of oxygen atoms on the vibrational relaxation of oxygen. *The 11th Symposium on Combustion*, Pittsburg, CA. p. 67-74.

Landau, L. and Teller, E. (1936). Theory of sound dispersion. *Physikalische Zeitschrift der Sowjetunion*, 10, 34-43.

Lee, S. H. (1986). Electron impact vibrational excitation in the flow field of aero assisted orbital transfer vehicles. In J. N. Moss and C. D. Scott, eds. *Progress in Astronautics and Aeronautics, Vol. 103: Thermophysical aspects of Re-entry Flows*. New York, NY: American Institute of Aeronautics and Astronautics. pp. 197-224.

Nagamatsu, H. T. (1959). *Real Gas Effects in Flow Over Blunt Bodies at Hypersonic Speeds* (Report NO. 59-RL-2177). New York, NY: General Electric Research Laboratory.

Park, C. (1989). *A Review of Reaction Rates in High Temperature Air*. AIAA Paper, 89, 1740.

Thivet, F. (1989). *Modeling of Nonequilibrium of Vibration in Reactive Flow* (Management Report). Laboratory of Molecular and Macroscopic Combustion, CNRS/ECP.

Van Leer, B. (1982). Flux vector splitting for the Euler Equations. *Lecture Notes in Physic*s, 170, 507-512.

Wray, K. L. (1962). Shock tube study of the vibrational relaxation of nitric oxide. *Journal of Chemical Physics*, 36, 2597-2603.